Journal of Applied Polymer Science

Thermotropic Glazings for Overheating Protection. I. Material Preselection, Formulation, and Light-Shielding Efficiency

Andreas Weber,[1] Katharina Resch[2]

[1]Polymer Competence Center Leoben GmbH, Roseggerstrasse 12, 8700 Leoben, Austria

[2]Department Polymer Engineering and Science, University of Leoben, Otto Glöckel-Strasse 2, 8700 Leoben, Austria

Correspondence to: K. Resch (E-mail: katharina.resch@unileoben.ac.at)

ABSTRACT: This article presents a systematic strategy for formulation and optimization of thermotropic layers for overheating protection purposes. Specifically, thermotropic systems with fixed domains (TSFD) which consist of a thermotropic additive finely dispersed in a matrix material are considered. Based on systematic material (component) preselection regarding thermoanalytical characteristics and refractive indices, numerous thermotropic layers were formulated. TSFD with thermoplastic matrix were produced by compounding and compression molding. TSFD with resin matrix were produced by UV curing. The thermotropic layers were analyzed as to solar optical properties, threshold temperature, switching process and residual transmittance in the opaque state applying UV/Vis/NIR spectrometry equipped with a heating stage. Best performing materials exhibited solar hemispheric transmittance in the range of 72.2–84.5% and between 59.6 and 83.7% in the clear and opaque state, respectively. Threshold temperatures between 45 and 75°C were realized. Refractive index difference between matrix and additive and solar hemispheric transmittance displayed a close correlation. Hence, refractometry was shown to be an appropriate tool for material preselection. Furthermore, investigations revealed a close correlation of thermal transitions of thermotropic additives recorded by differential scanning calorimetry and threshold temperatures of thermotropic layers formulated therewith. However, thermotropic layers formulated so far have to be optimized with respect to light-shielding performance for efficient overheating protection. © 2013 Wiley Periodicals, Inc. J. Appl. Polym. Sci. **2014**, *131*, 39950.

KEYWORDS: differential scanning calorimetry (DSC); optical and photovoltaic applications; optical properties; photochemistry; spectroscopy

Received 10 July 2013; accepted 10 September 2013

DOI: 10.1002/app.39950

INTRODUCTION

Thermotropic glazings change their light transmittance from transparent to opaque upon reaching a certain threshold temperature reversibly.[1,2] Their application in passive and active solar energy utilization allows tailoring solar gains to climatic, user and/or technical demands.[3,4] Design of façades with thermotropic glazings enhances thermal and visual comfort of building occupants and reduces primary energy consumption for space heating/cooling and artificial daylighting due to solar contributions.[3,5–8] Design of solar thermal collectors with thermotropic glazings limits collector stagnation temperature to temperatures below 130°C.[4] Limiting the stagnation temperature of solar thermal flat-plate collectors to values below the long-term service temperature of cost-efficient plastics (~125°C) allows for utilization of these polymers as absorber material, thus yielding significant cost-reduction potential.[4] Application of thermotropic glazings in solar thermal collectors at the glazing unit or the absorber requires threshold temperatures of 55–60°C and 75–80°C, respectively.[4] To maintain efficient overheating protection for a solar thermal collector, solar hemispheric transmittance has to change from >85% in the transparent state to <60% in the opaque state.[4] Such global requirements cannot be derived for window applications due to complex situation of glazing in the architectural context (building usage, lighting requirements, local climate, orientation, structural design, etc.).[1,7–10] Furthermore, materials shall exhibit a rapid and steep switching process within a small temperature range.[4] Among different thermotropic materials, thermotropic systems with fixed domains (TSFD) exhibit probably the highest potential for these applications.[11] Ease of adjustment of switching threshold, high reversibility, long-term stability and a steep switching process with low hysteresis are significant advantages of TSFD.[12] The key for the superior performance of TSFD is their inherent persistent two-phase material structure: TSFD consist of a thermotropic additive that is finely dispersed in a polymeric matrix material.[1,3] Below the threshold temperature, the refractive indices of both components are almost equal, resulting in a transparent appearance of the TSFD.[1] With increasing temperature a phase transition (e.g., melting) of the

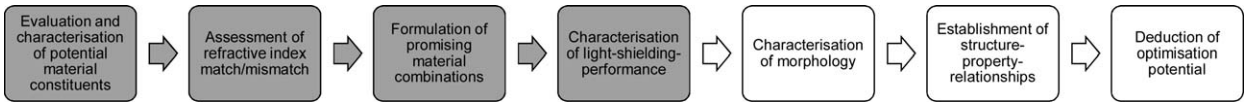

Figure 1. Systematic material formulation strategy.

thermotropic additive causes the refractive index difference of matrix and additive to change steeply.[1,3] Thus incident radiation is multiply scattered at the interfaces of the matrix and the scattering domains formed by thermotropic additive.[13] Consequently, the layer turns opaque.

Nevertheless, TSFD reported in scientific literature so far do not meet the performance requirements described above.[3,4,14–16] However, the material portfolio investigated so far is limited.[12] Thus, the overall objective of this study is to perform an extensive evaluation of the overheating protection potential of combinations of numerous different matrix materials and thermotropic additives. Therefore, a systematic material formulation strategy is applied. First, a comprehensive polymer-physical characterization of candidate TSFD components is carried out. Subsequently, various TSFD are formulated and characterized as to their performance characteristics. Finally, the overheating protection characteristics of the TSFD are related to component properties.

SYSTEMATIC MATERIAL FORMULATION STRATEGY

Refractive index difference of matrix and additive and TSFD morphology are of paramount importance for scattering performance and thus overheating protection performance of TSFD.[5] Hence, for the development of novel TSFD a systematic material formulation strategy—which is depicted in Figure 1—has been established to account for these factors. The strategy comprises seven different steps. Steps which are addressed within the present article are colored gray. First, a comprehensive literature review concerning material properties is carried out to evaluate candidate matrix materials and thermotropic additives: Matrix materials exhibit preferably high transition temperatures (glass transition, melting), high transmittance and a refractive index as low as possible. Thermotropic additives must display a thermal transition—preferably melting—between 30 and 105°C along with a rapid and steep change of refractive index. Subsequently, a comprehensive polymer-physical characterization of candidate matrix materials and thermotropic additives with regard to thermal, thermomechanical and optical properties is carried out. In the second step appropriate combinations of candidate matrix materials and thermotropic additives are identified by assessment of refractive index match/mismatch. Based on this evaluation procedure promising TSFD are formulated and characterized as to light-shielding efficiency, switching characteristics and threshold temperature. Finally, a comprehensive characterization of morphology (scattering domain size, shape, distribution) is carried out and structure-property-relationships are established. Based on these interrelationships, the optimization potential of the TSFD is deduced. However, these final steps are addressed in a subsequent publication.[17]

As the steps outlined above have different requirements with regard to the desired information on polymer-physical characteristics of the materials, it is considered more appropriate to present the experimental details of each step of the systematic material formulation strategy in the section where they apply (instead of a cumulative experimental part).

Evaluation and Characterization of Potential Material Constituents

Materials. For matrix materials, the material selection focused on polymers exhibiting the following desired properties. The transition temperature of polymers—glass transition for amorphous polymers and melting for semicrystalline polymers—was required to be as high as possible but at least as high as 120°C. Furthermore, high transparency was desirable. The transparency requirement was most likely to be fulfilled by polymers lacking intrinsic scattering domains (i.e., crystallites). Polymers lacking crystallites like amorphous polymers (thermoplastic resins, thermosets) were most promising but also semicrystalline thermoplastic resins exhibiting crystallites with reduced size and thus less scattering (so called "micro-crystalline" thermoplastic resins) were considered. Besides that, materials not prone or even less than other materials to UV-induced degradation were preferred, including UV-stabilized material grades. That was also important because initially nonpolymeric resin matrices had to be UV curable. Furthermore, a proper match of refractive index of matrices and potential thermotropic additives at room temperature was required. Especially acrylic-esters are recognized to withstand UV irradiation.[18] Thus, focus was on acrylic polymers, but also UV-stabilized polyamide and polycarbonate were considered.

For the thermotropic additives—as outlined before—a thermal transition in the desired temperature range between 30 and 105°C accompanied by a steep change in refractive index of the thermotropic additive was desirable. As outlined before, a proper match of refractive index of matrices and potential thermotropic additives at room temperature was required. As acrylic polymers have refractive indices around 1.5,[19] focus was on potential thermotropic additives having a refractive index around 1.5 at room temperature also.

A total of seven matrix materials were selected, which are listed in Table I. In case the exact material composition was not disclosed by the supplier, the product name of the material is mentioned instead. The material portfolio comprised three thermoplastics: A poly(methyl methacrylate) (PMMA: Plexiglas FT15, Evonik Röhm GmbH; M1), a semicrystalline polyamide PA PACM 12 (PA; Trogamid CX9703, Evonik Degussa GmbH; M2) and a polycarbonate (PC; Makrolon ET3127, Bayer Materials Science AG; M3). Four different UV-curable resin systems were employed: A hexa-functional aromatic urethane acrylate (based on oligomer Ebecryl 220; M4), a di-functional aliphatic urethane acrylate (based on oligomer Ebecryl 284; M5), a di-functional epoxy acrylate (based on oligomer Ebecryl 600; M6), and a tetra-functional polyester acrylate (based on oligomer

Table I. Candidate Matrix Materials

Matrix	Material type
M1	Poly(methyl methacrylate)
M2	Polyamide
M3	Polycarbonate
M4	Aromatic urethane acrylate
M5	Aliphatic urethane acrylate
M6	Epoxy acrylate
M7	Polyester acrylate

Ebecryl 800; M7). Ebecryl resins were provided by Allnex Belgium SA/NV (former Cytec Surface Specialites).

In Table II, the selected thermotropic additives are listed (all materials are technical grades and probably only a small fraction of ingredients is disclosed by suppliers, thus exact chemical structures cannot be presented). The material portfolio comprised a low (A1) and high molecular paraffin wax (A2), which were the most nonpolar additives investigated. The latter is a Fischer-Tropsch wax. Furthermore, fatty acids and their derivatives were considered: fatty acid mixture (A3), glycerine tristearate (A4), hydrogenated castor oil (A5; main component: glycerine trihydroxystearate), pentaerythritol tetrastearate (A6), hydroxystearic acid (A7), glycerine monostearate (A8), a montan wax (A9) and again a hydrogenated castor oil (A10; main component: glycerine trihydroxystearate). A5 and A10 were provided by different suppliers. In general, fatty acids and fatty acid esters are more polar than paraffin waxes because of their carboxyl group. However, within the group of fatty acids and derivatives one may discriminate between more and less polar substances: The longer the lipophilic tails of the fatty acids or alcohols are, the less polar the ester will be for example. This applies for instance for montan wax (A8) with esters of montanic acid (a C_{28} carboxylic acid) as an important component. On the contrary, fatty acids or derivatives (including their esters) of fatty acids with shorter lipophilic chains compared to montanic acid or with additional polar groups on these are considered more polar. A proper example would be A7, a C_{16} carboxylic acid chain with a hydroxyl moiety attached to the lipophilic tail. As a rule of a thumb: the longer the alkyl moiety, the less polar a molecule is (and lipophilicity increases).

Furthermore, various polymers like a copolymer of ethylene (E) and glycidyl methacrylate (GMA) (Lotader AX8840, Arkema; A11), a terpolymer of E, methyl acrylate (MA) and GMA (Lotader AX8900, Arkema; A12), a terpolymer of E, butyl acrylate (BA) and maleic anhydride (MAH) (Lotader 3410, Arkema; A13), two terpolymers of E, MA and MAH with varying contents of MA and MAH (Lotader 3430, Arkema; A14; Lotader 4503, Arkema; A15), a terpolymer of E, ethyl acrylate (EA) and MAH (Lotader 4700, Arkema; A16), two copolymers of E and vinyl acetate (VA) with lower and higher VA-content (Evatane 28-03, Arkema; A17; Evatane 33–45, Arkema; A18), a copolymer of E and MA (Elvaloy 1330AC, DuPont de Nemours (Deutschland) GmbH; A19), a polystyrene (PS) (Empera 116N, Ineos Nova; A20), a glycol-modified poly(ethylene terephthalate) (Eastar 6763, Eastman; PETG) (A21), naphthalene (A22), sodium tetraborate decahydrate (A23) and sodium sulfate decahydrate (A24) were selected.

Experimental. ***Specimen preparation.*** For dynamic mechanical analysis (DMA), UV/Vis/NIR measurements and determination of refractive index plate-like specimens were prepared. Thermoplastics were compression molded to 800 µm thick plates on a press P200PV (Dr. Collin GmbH, Ebersberg, DE). Plates from UV-curable resin systems were prepared by mixing 57 wt % oligomers, 40 wt % reactive diluent trimethylol propane triacrylate (TMPTA) and 3 wt % photoinitiator (blend of benzophenone and 1-hydroxycyclohexyl phenyl ketone). The mixtures were poured in the intervening space between two glass panes, which were sealed around the edge. Layers were cured by UV-radiation (dose: 2.1 J/cm^2) from a Light Hammer 6 equipped with a mercury-lamp and a LC6E Benchtop Conveyor (Fusion UV Systems, Gaithersburg, MD). Free standing layers with a thickness of 900 µm were obtained after removal of the glass panes.

Differential scanning calorimetry. The thermal transitions of candidate matrix materials and thermotropic additives were determined by differential scanning calorimetry (DSC). Thermograms were recorded in static air on a DSC822^e (Mettler Toledo GmbH, Schwerzenbach, CH). For samples exhibiting a glass

Table II. Candidate Thermotropic Additives

Additive	Material type
A1	Paraffin, low-molecular weight
A2	Paraffin, high-molecular weight
A3	Fatty acids (mixture)
A4	Glycerine tristearate
A5	Hydrogenated castor oil[a]
A6	Pentaerythritol tetrastearate
A7	Hydroxystearic acid
A8	Glycerine monostearate
A9	Fatty acid ester
A10	Hydrogenated castor oil[a]
A11	E-*co*-GMA (8%)
A12	E-*co*-MA (24%)-*co*-GMA (8%)
A13	E-*co*-BA (17%)-*co*-MAH (3.1%)
A14	E-*co*-MA (16%)-*co*-MAH (3.1%)
A15	E-*co*-MA (20%)-*co*-MAH (0.3%)
A16	E-*co*-EA (29%)-*co*-MAH (1.3%)
A17	E-*co*-VA(28%)
A18	E-*co*-VA (33%)
A19	E-*co*-MA (30%)
A20	PS
A21	PETG
A22	Naphthalene
A23	Sodium tetraborate decahydrate
A24	Sodium sulfate decahydrate

[a] Different suppliers.

Table III. Applied Strain Amplitudes for DMA and Measurement Temperature Range

Matrix	Strain amplitude (μm)	Start temperature (°C)	End temperature (°C)
M1	5	−50	180
M2	5	−50	200
M3	5	−50	180
M4	4	−80	160
M5	4	−80	160
M6	4	−80	160
M7	5	−80	160

transition only, a heating rate of 20 K min^{-1} was used in order get a distinct glass transition signal. A heating rate of 10 K min^{-1} was applied to samples exhibiting melting to be able to discriminate between individual transitions more clearly (e.g., between solid phase transition and melting which probably would be displayed as a single peak upon application of higher heating rates). In general, high heating rates are recommended to detect effects of small magnitude (like glass transitions) but resolution is decreased compared to lower heating rates.[20] The sample mass was 10 ± 1 mg. Glass transition temperature and melting temperature were evaluated as mid-point temperature and peak temperature, respectively, according to ISO 11357-1 from the second heating run. The data were averaged over two measurements.

Dynamic mechanical analysis (DMA). Thermomechanical properties of films produced from the different matrix resins M1 to M7 were characterized by dynamic mechanical analysis (DMA) on a DMA/SDTA 861[e] (Mettler Toledo GmbH, Schwerzenbach, CH). Rectangular specimens (17 mm × 4 mm × 0.8–0.9 mm) were cut from plate-like samples with a saw Diadisc 5200 (Mutronic Präzisionsgerätebau GmbH & Co. KG, Rieden am Forggensee, DE). The gauge length was 9 mm. DMA was carried out in tensile mode applying sinusoidal strain amplitude at a frequency of 1 Hz. Strain amplitudes (determined by strain-sweep procedure) and measurement temperature ranges applied for the different material types are summarized in Table III. Scans were run with a heating rate of 3 K min^{-1}. From DMA, storage modulus (E'), loss modulus (E'') and loss factor (tan δ) curves, were generated as a function of specimen temperature. The temperature at the maximum in loss modulus was taken as the glass transition temperature. Thermomechanical properties were averaged over two measurements.

UV/Vis/NIR spectrometry. Solar transmittance, reflectance and absorptance of the matrix materials were determined applying UV/Vis/NIR spectrometry. A double beam UV/Vis/NIR spectrophotometer Lambda 950 (Perkin Elmer, Waltham, MA) equipped with an Ulbricht-sphere (diameter 150 mm) was utilized. For the given measurement apparatus the radiation passing through (transmittance) or being reflected (reflectance) from the specimen outside a cone of ~5° relative to the incident beam direction was defined as diffuse (scattered) component. Hemispheric and diffuse transmittance and reflectance were recorded at normal incidence in the spectral region from 250 to 2500 nm. The integral solar transmittance and reflectance were determined by weighting the recorded spectral data in steps of 5 nm by the AM1.5 global solar irradiance source function. A single determination was carried out for each material.

Refractometry. Refractive indices as a function of temperature of matrix materials and thermotropic additives were determined on an Abbé-type refractometer AR4 (A. Krüss Optronic GmbH, Hamburg, DE) equipped with a water bath Ecoline E306 (Lauda Dr. R. Wobser GmbH & Co. KG, Lauda-Königshofen, DE) to maintain operation temperature. Measurements were conducted in a temperature range between ambient temperature and a maximum of 90°C. A LED illumination unit with a wavelength of 589 nm was used. The temperature of the prisms was recorded with a two-channel temperature measurement instrument T900 (Dostmann electronic GmbH, Wertheim-Reicholzheim, DE) equipped with a precision K-type thermocouple. Measured prism temperatures were crosschecked by measurement of the refractive index of water as a function of temperature and comparison with tabulated values.[21] The crosscheck confirmed the accuracy of temperature values detected by the two-channel instrument. Refractive indices were averaged over three measurements.

Table IV. Basic Characteristics of Matrix Materials

Matrix	T_m (DSC) (°C)	T_g (DSC) (°C)	T_g (DMA) (°C)	τ_{nh} (%)	ρ_{nh} (%)	α (%)	n^D_{29} (1)
M1	–	125	122	85	8	7	1.502
M2	250	131	128	83	7	10	1.516
M3	–	147	148	84	8	8	1.587
M4	–	–[a]	−6	84	8	8	1.525
M5	–	–[a]	24	84	8	8	1.512
M6	–	–[a]	17	84	8	8	1.551
M7	–	–[a]	−2 to 10[b]	85	8	7	1.521

Melting temperatures detected by DSC (T_m), glass transition temperatures (T_g) detected by DSC and DMA, solar hemispheric transmittance (τ_{nh}), solar hemispheric reflectance (ρ_{nh}), absorptance (α), and refractive index at 29°C (n^D_{29}).
[a] Not detectable.
[b] Broad plateau in E''-curve detected.

Table V. Transition Temperatures, Kind of Transition, Transition Interval of Candidate Thermotropic Additives Detected by DSC Along with Refractive Indices Below (n^D_{29}) and Above ($n^D_{T>T(transition)}$) the Transition Temperature and Classification of Eligibility for TSFD Formulation

Additive	Transition temperature (°C)	Kind of transition	Transition interval ΔT (°C)	$n^D_{29°C}$ (1)	$n^D_{T>T(transition)}$ (1)	Classification
A1	35/55	Solid phase transition/melting	31/22	1.497	1.435	Pass
A2	86	Melting	37	1.514	1.435	Pass
A3	64	Melting	32	1.529	1.434	Pass
A4	51/54/61	Melting/recrystallization/ melting	18/3/9	1.495	1.445	Pass
A5	59/80/87	Solid phase transition/solid phase transition/ melting	19/17/10	1.503	1.462	Pass
A6	47/57/62	Solid phase transition/solid phase transition/melting	-/27/7	1.503	1.449	Pass
A7	55/78	Melting/melting	23/26	1.500	1.443	Pass
A8	52/60	Solid phase transition/melting	30	1.502	1.448	Pass
A9	81	Melting	53	1.506	1.447	Pass
A10	61/80/86	Solid phase transition/solid phase transition/ melting	27/16/9	1.502	1.460	Pass
A11	106	Melting	>50	1.507	1.478	Pass
A12	63	Melting	>50	1.484	1.459	Pass
A13	90	Melting	>50	1.493	1.459	Pass
A14	87	Melting	>50	1.495	1.460	Pass
A15	82	Melting	>50	1.493	1.458	Pass
A16	66	Melting	>50	1.485	1.454	Pass
A17	77	Melting	>50	1.488	1.458	Pass
A18	63	Melting	>50	1.482	1.455	Pass
A19	55[a]	Melting	>50	1.487	1.460	Pass
A20	90	Glass transition	30	1.586	1.574	Pass
A21	80	Glass transition	24	1.565	1.551[b]	Pass
A22	85	Melting	12			Reject
A23	77/99	Melting/evaporation	55			Reject
A24	-	-	No transition detectable			Reject

[a] No distinct maximum detectable.
[b] Transition not completed at maximum operation temperature of refractometer.

Results. Table IV summarizes melting temperature, glass transition temperature, solar-optical properties at ambient temperature and refractive index at 29°C of matrix materials investigated. The application temperature limits for amorphous and semicrystalline thermoplastic materials from a thermomechanical point of view are below glass transition and melting temperature, respectively.[22] Thermosets are applicable up to their decomposition temperature.[22] For semicrystalline material M2 a melting peak at 250°C was detected. DSC and DMA yielded glass transitions around 125, 130, and 148°C for thermoplastic matrix materials M1, M2, and M3. No decomposition was detected. Whereas glass transition was not observed by DSC for UV-curable resin systems M4 to M7, DMA revealed glass transitions at −6, 24, and 17°C of materials M4, M5, and M6, respectively. For material M7 a broad plateau in E''-curve was ascertained. Thus an exact designation of glass transition temperature was not possible for this material. The plateau ranged from −2 to 10°C. For systems M4 to M7, no decomposition

was detected up to the maximum investigation temperatures of 150 and 160°C in DSC and DMA, respectively.

Matrix materials have to be mechanically stable during operation. Hence, all matrix materials are appropriate for collector application (stagnation temperature of collector ~128°C, Ref. 4) according to the criteria mentioned above, except for M1. For window applications all materials are appropriate (this estimation is based on the maximum recorded air-temperature on earth, which is ~57°C, Ref. 23).

Refractive indices of matrix materials M1 to M7 varied between 1.502 and 1.587. Solar hemispheric transmittance and reflectance ranged from 83 to 85% and 7 to 8%, respectively. Absorptance varied between 7 and 10%. However, for maintaining high efficiency of a solar thermal flat-plate collector equipped with thermotropic overheating protection glazing, a transmittance of at least 85% is required in the clear state of the TSFD.[4] Transmittance can be increased by reducing the layer thickness on the one hand side. On the other hand side, reflectance can be minimized (i.e., increase in transmittance) by reducing refractive index of matrix material.[24] However, the latter approach would require the replacement of the matrix material.

Table V summarizes the transition temperatures, the transition temperature interval and the kind of transition of thermotropic additives. Furthermore, Table V comprises refractive indices of the thermotropic additives below (at 29°C) and above the phase transition temperature. Solid phase transitions and subsequent melting upon increasing temperature were detected for additives A1,[25–29] A5, A6,[30] A8,[31–33] and A10. Melting of two polymorphs with recrystallization between these melting processes were evident for additive A4.[34–37] Additive A7 displayed two melting peaks. The lower temperature peak was attributed to melting of impurities.[38] Solely melting was detected for additives A2,[26] A3, A9, and A11 to A19. DSC thermograms revealed glass transitions for additives A20 and A21.

Although additive A22 exhibited a rather narrow endothermic peak at 85°C, naphthalene was rejected from further investigations due to high degree of supercooling (crystallization at 58°C). Furthermore, it is suspected to be carcinogenic.[39] For additive A23 an endothermic double peak with maxima at 77 and 99°C was ascertained in the first heating run. The first maximum correlated with melting of the salt hydrate. The second peak was ascribed to evaporation of water. Because of lack of water and thus lacking formation of salt hydrate, no transition was observed in the second heating run within the investigated temperature range (20–130°C). Most salt hydrates display separation of water and salt during melting yielding irreversible behavior during a melting/solidification cycle.[40,41] Additive A24 was used as received. It displayed no thermal transition between −20 and 80°C, although a melting point of 32°C is reported.[41]

Refractive indices of additives A1 to A21 ranged between 1.482 and 1.586 at 29°C. Additives A1 to A19 exhibited rather distinct changes (≥0.025) in refractive index when exceeding the transition temperature. For additives A20 and A21 only minor reductions (~0.01) were achieved. The refractive index $n^{D}_{T > T(transition)}$ of additive A21 was recorded at the maximum operation temperature (90°C) of the refractometer. Transition temperatures given in Table V already allow for material classification in terms of applicability. Hence, thermotropic additives exhibiting distinct or transient phase transitions in the temperature range between 30 and 105°C are labeled "pass" in Table V. Those displaying no phase transition or irreversible effects are labeled "reject." Therefore, additives A22 to A24 were excluded from further investigations and are hence not displayed in subsequent tables and figures.

Assessment of Refractive Index Match/Mismatch

In Figures 2 and 3, the refractive index difference between matrix and additive below (black) and above (gray) the transition temperature of the additive is presented for thermoplastic matrix materials (M1, M2, and M3) and for UV-curable matrix materials (M4, M5, M6, and M7), respectively. For additives exhibiting phase transitions at temperatures equal or higher than the maximum operation temperature of the refractometer

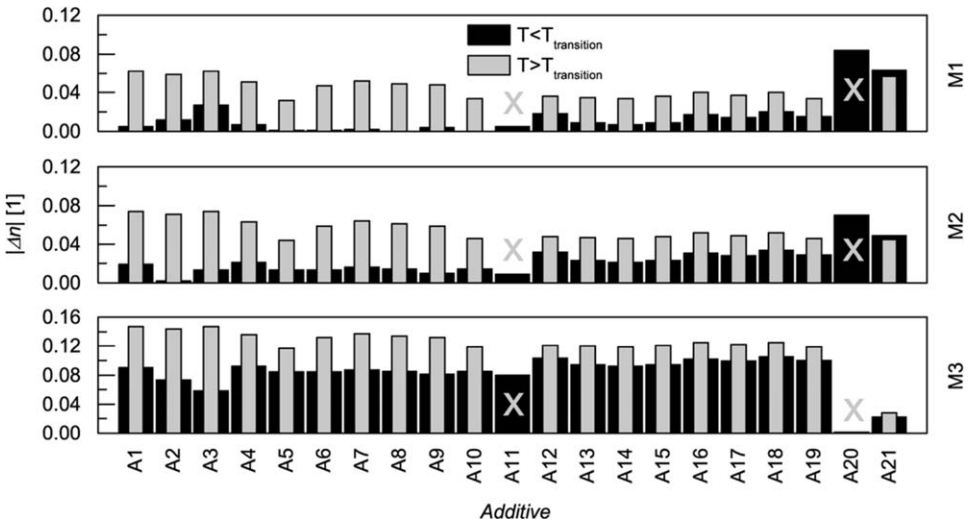

Figure 2. Refractive index difference between matrix and additive below (at 29°C; black) and above (at $T > T_{transition}$; gray) the transition temperature of the additive for thermoplastic matrix materials M1, M2, and M3. Gray symbol (x) denotes excluded data.

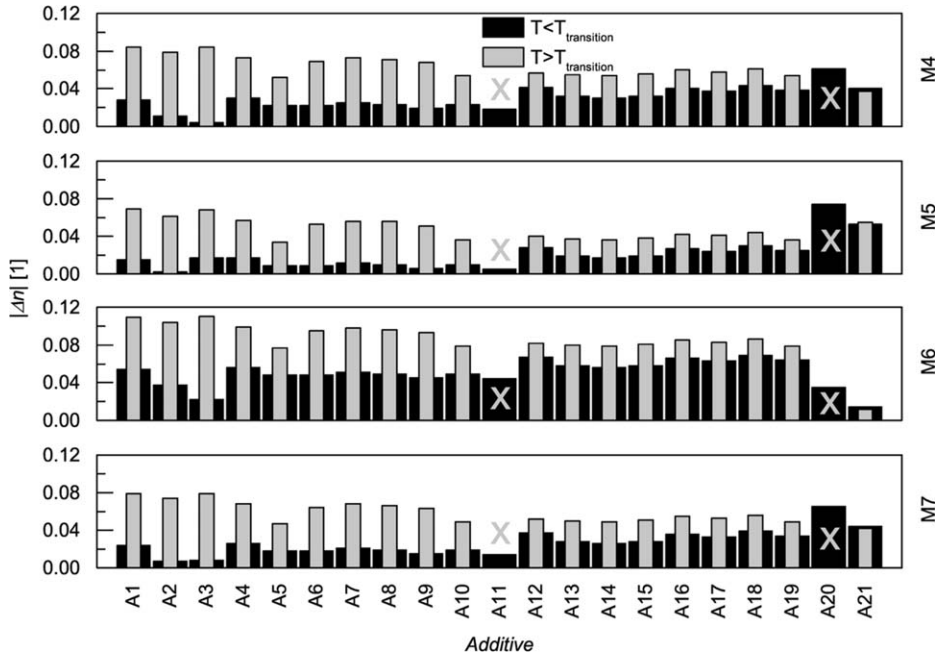

Figure 3. Refractive index difference between matrix and additive below (at 29°C; black) and above (at $T > T_{transition}$; gray) the transition temperature of the additive for UV-curable matrix materials M4, M5, M6, and M7. Gray symbol (x) denotes excluded data.

(90°C), refractive index data are presented for 29°C only to avoid misleading interpretation of refractive index difference at temperatures above the transition temperature. For additives A11 to A19, which exhibited a broad transition temperature range $\Delta T > 50$°C (see Table V) with peak temperatures up to 106°C and additives A20 and A21 with glass transitions close to 90°C refractive index data were selected as follows: If the vast majority of the transition was already done at the maximum measurement temperature of the refractometer (90°C), refractive index difference data were included. At 90°C this was true for all materials except for additives A11 and A20 (see "Results" section). Thus, their data were excluded at 90°C.

Refractive index difference between matrix material and thermotropic additive below the phase transition temperature of the additive has to be as low as possible.[5] Thus, if the refractive index difference between matrix and additive was smaller than 0.02 below (29°C) the phase transition temperature of the thermotropic additive, the material combination was categorized as "appropriate." Combinations of matrix and additive with refractive index difference from 0.02 to lower than 0.03 at 29°C were categorized as "appropriate with limitation." Matrix/additive combinations not complying with these criteria were rejected. When exceeding the phase transition temperature, refractive index difference is required to be as high as possible.[5] Thus, combinations displaying a refractive index difference $\geq$0.03 above the phase transition temperature of the additive were considered as "appropriate," whereas those with a refractive index difference <0.03 were considered as "inappropriate" and therefore rejected. As to the nomenclature, a system composed of Matrix M1 and Additive A1 is named M1A1.

According to these criteria, material combinations M1A1, M1A2, M1A4 to M1A10, M1A12 to M1A17, M1A19, M2A1 to M2A3, and M2A5 to M2A10 were appropriate for formulation. Material combinations M1A11, M2A11, and M3A20 showed refractive index difference <0.02 at 29°C, which may yield high transmittance at ambient conditions. Thus, regardless of omitted refractive index difference at high temperatures (omission due to technical reasons as pointed out above), these material combinations were considered for formulation. Combinations M1A3, M1A18, M2A4, M2A13 to M2A15, M2A17, and M2A19 were appropriate with limitation for formulation according to the criteria defined above. Material combinations M1A20, M1A21, M2A12, M2A16, M2A18, M2A20, M2A21, and M3A1 to M3A19 were rejected from further investigations due to inappropriate refractive index difference. Combination M3A21 displayed refractive index differences of 0.022 and 0.028 at temperatures below and above the glass transition, respectively. Nevertheless, this combination was accepted for formulation due to not completed thermal transition of the additive at the maximum operation temperature of the refractometer.

Material combinations M4A2, M4A3, M4A9, M5A1 to M5A10, M5A13 to M5A15, M7A2, M7A3, M7A5, M7A6, and M7A8 to M7A10 were appropriate for formulation according to the criteria defined above. Material combinations M4A11, M5A11, and M7A11 exhibited refractive index difference <0.02 at 29°C, respectively. Low refractive index differences of combinations M4A11, M5A11, and M7A11 were likely to yield high transmittance at ambient conditions. Thus, regardless of omitted refractive index difference at high temperatures (omission due to technical reasons as pointed out above), these material combinations were considered for formulation. Combinations M4A1, M4A5 to M4A8, M4A10, M5A12, M5A16, M5A17, M5A19, M6A3, M7A1, M7A4, M7A7, and M7A13 to M7A15 were considered appropriate with limitation for formulation. Material

Table VI. Actually Formulated TSFD

	M1	M2	M3	M4	M5	M6	M7
A1	+	−	−	+	+	+	+
A2	+	+	−	+	+	+	+
A3	−	+	−	+	+	+	+
A4	−	−	−	−	+	−	+
A5	−	+	−	+	+	−	+
A6	−	+	−	+	+	−	+
A7	−	−	−	+	+	−	+
A8	−	−	−	+	+	−	+
A9	−	−	−	+	+	−	+
A10	−	−	−	+	+	+	+
A11	+	+	−	−	−	−	−
A12	−	−	−	−	−	−	−
A13	−	−	−	−	−	−	−
A14	−	−	−	−	−	−	−
A15	−	−	−	−	−	−	−
A16	−	−	−	−	−	−	−
A17	−	−	−	−	−	−	−
A18	−	−	−	−	−	−	−
A19	−	−	−	−	−	−	−
A20	−	−	+	−	−	−	−
A21	−	−	+	−	−	−	−

+, Materials formulated; −, materials not formulated.

combinations M4A4, M4A12 to M4A21, M5A18, M5A20, M5A21, M6A1, M6A2, M6A4 to M6A21, M7A12, and M7A16 to M7A21 were rejected from formulation due to inappropriate refractive index difference.

Formulation of Promising Material Combinations

TSFD with thermoplastic matrices were manufactured at APC Advanced Polymer Compounds (Gai, AT) by melt blending on a compounder Coperion ZSK 26 Mcc (Coperion GmbH, Stuttgart, DE). From the compound 800 μm thick plates were obtained by compression molding on a press P200PV (Dr. Collin GmbH, Ebersberg, DE). Thermotropic layers based on UV-curable resin matrix were prepared by dissolving the thermotropic additive above its transition temperature in the photo-crosslinkable matrix solution, which consisted of 57 wt % oligomers, 40 wt % reactive diluent TMPTA and 3 wt % photoinitiator (blend of benzophenone and 1-hydroxycyclohexyl phenyl ketone). The dissolutions were poured in the intervening space between two glass panes, which were sealed around the edge. Afterward, the samples were stored at ambient temperature for 10 min allowing for precipitation of the additive. Next the mixtures were cured by UV-radiation (dose: 2.1 J cm^{-2}) from a Light Hammer 6 equipped with a mercury-lamp and a LC6E Benchtop Conveyor (Fusion UV Systems). Free standing layers with a thickness of 900 μm were obtained after removal of the glass panes. TSFD based on UV-curable resin matrix were annealed at the temperature at which mixing of the matrix solution with the corresponding additive was carried out. For both, thermoplastic and resin based TSFD, the theoretical additive concentration was 5 wt %.

Matrix/additive combinations which were chosen for formulation of TSFD are depicted in Table VI. Selection was mainly based on refractive index data discussed above. For combinations of matrix M1 and ethylene co- and terpolymer additives A11 to A19 exhibiting a moderate difference in refractive index above the transition temperature, M1A11 was compounded to represent this material class (ethylene co- and terpolymers). M1A11 showed the best refractive index match of the components below the transition temperature. Furthermore, additive A11 was the only ethylene co- or terpolymer that fitted matrix M2 properly with regard to refractive index at low temperatures. Furthermore, combinations M1A1, M1A2, M2A2, M2A3, M2A5, M2A6, M3A20, and M3A21 were compounded. Materials M1A2, M1A11, M2A2, M2A6, M2A11, M3A20, and M3A21 were processable properly. However, compounding of matrix M1 and additive A1 resulted in partial liquid leakage of additive at machine joints due to large differences in melt viscosity of the components. Large differences in viscosity of polymer melt and molten additives led to inaccurate miscibility of matrix M2 and additives A3 and A5 also. TSFD based on UV-curable matrix M4A1 to M4A3, M4A5 to M4A10, M5A1 to M5A10, M6A3, and M7A1 to M7A10 were formulated successfully. Combinations M6A1, M6A2, and M6A10, which were inappropriate for formulation due to high refractive index difference at ambient temperature, were investigated additionally to study the effect of refractive index difference on solar optical properties of TSFD. Whereas, mixtures of UV-curable matrix materials and additives A3 to A10 were stable during processing, mixtures of M4, M5, M6, or M7 with additives A1 or A2 exhibited limited miscibility, sometimes resulting in separation of macroscopic additive domains with dimensions in the range of millimeters. For any system with UV-curable resin matrix (M4 to M7), additives A11 to A21 were rejected from formulation due to a lack of processability.

Characterization of Light-Shielding Performance

Experimental. Solar transmittance as a function of temperature, threshold temperature and switching process of TSFD were determined applying UV/Vis/NIR spectrometry. Deviant from the procedure described in "UV/Vis/NIR spectrometry" section, the spectrophotometer was adapted by a heating stage to adjust sample temperature within a range from ambient temperature to maximum 115°C. Measurements were performed in steps of 5 K for one sample of each TSFD. Replicate measurements (samples two and three) were conducted at ambient temperature and at a temperature above the switching threshold of the respective TSFD. Prior to measurement, the samples were allowed to equilibrate for 5 min at the selected temperature. The heating stage was equipped with a control system consisting of a heating stage-internal J-type thermocouple as temperature sensor and the control unit HS-W-35/M (Heinz Stegmeier Heizelemente HS-Heizelemente GmbH, Fridingen, DE). Within the heating stage the sample was positioned in close proximity of the port hole of the Ulbricht-sphere. In situ front- and backside sample surface temperatures as a function of set-point value of the control unit were recorded on a prototype sample with a

Table VII. Threshold Temperature T_{th}, Major Switching Interval ΔT_{major}, Mean of Solar Hemispheric and Diffuse Transmittance Below and Above the Threshold Temperature of TSFD Based on Thermoplastic Matrix (Empirical Standard Deviation in Brackets), and Test Variable t_d

			Solar transmittance below threshold temperature (%)		Solar transmittance above threshold temperature (%)			
TSFD	T_{th} (°C)	ΔT_{major} (°C)	Hemisph.	Diffuse	Hemisph.	Diffuse	t_d	Remarks
M1A1	45	15	36.7 (0.7)	36.4 (0.6)	53.3 (1.6)	52.0 (1.4)	26.5	Highly sign. incr.
M1A2	65	30	37.0 (1.4)	37.0 (1.4)	66.1 (5.6)	65.9 (5.1)	11.8	significant incr.
M1A11	75	20	39.6 (2.8)	35.4 (1.6)	64.6 (3.2)	55.9 (1.7)	51.5	Highly sign. incr.
M2A2	70	40	46.2 (2.5)	44.1 (2.6)	61.6 (13.6)	59.7 (12.0)	2.38	Insignificant
M2A6	55	10	59.9 (1.3)	38.2 (0.3)	71.8 (1.9)	44.2 (0.2)	35.0	Highly sign. incr.
M2A11	75	25	78.9 (0.8)	15.2 (1.1)	63.3 (1.2)	33.2 (2.3)	−52.2	Highly sign. decr. gradual switching process
M3A20	80	10	80.0 (0.9)	28.7 (3.1)	78.0 (4.5)	37.1 (1.9)	−0.94	Insignificant; intermediate reduction
M3A21	-	-	80.7 (1.1)	28.7 (4.8)	83.5 (0.3)	31.4 (3.5)	5.44	Indifferent incr.

two-channel temperature measurement instrument T900 (Dostmann electronic GmbH, Wertheim-Reicholzheim, DE) equipped with a precision K-type thermocouple. Sample temperature was assumed as the average of both recorded surface temperatures. Required set-point values to maintain average sample temperatures were calculated from a second order polynomial fit of the temperatures recorded in measurements of the prototype sample. Hemispheric and diffuse solar transmittance were averaged over three measurements. A dependent *t*-test for paired samples was applied to measured values of solar hemispheric transmittance to determine whether transmittance change was significant or not. Equality of mean values of solar hemispheric transmittance below ($\tau_{nh,\ cold}$) and above threshold temperature ($\tau_{nh,\ hot}$) was the null hypothesis (H_0: $\tau_{nh,\ hot} = \tau_{nh,\ cold}$ equal to $\tau_{nh,\ hot} - \tau_{nh,\ cold} = 0$).[42] H_0 was tested against alternative hypothesis H_A that $\tau_{nh,\ hot} < \tau_{nh,\ cold}$ (equal to $\tau_{nh,\ hot} - \tau_{nh,\ cold} < 0$) or $\tau_{nh,\ hot} > \tau_{nh,\ cold}$ (equal to $\tau_{nh,\ hot} - \tau_{nh,\ cold} > 0$).[42] H_A were tested one at a time, not at the same time. Thus a one-tailed *t*-test was applied. Test variable t_d was calculated according to Montgomery.[43] Test scenario 1: Testing H_0 ($\tau_{nh,\ hot} - \tau_{nh,\ cold} = 0$) against H_A ($\tau_{nh,\ hot} - \tau_{nh,\ cold} < 0$) led to rejection of H_0 if $t_d < -t_{1-\alpha;n-1}$. The symbol α denoted the alpha error and $n-1$ was the degree of freedom (in case of three pairs it was two). Test scenario 2: Testing H_0 ($\tau_{nh,\ hot} - \tau_{nh,\ cold} = 0$) against H_A ($\tau_{nh,\ hot} - \tau_{nh,\ cold} > 0$) led to rejection of H_0 if $t_d > t_{1-\alpha;n-1}$. Transmittance difference was classified according to Kleppmann[44]: H_0 not rejected at $\alpha = 0.05$ meant no significant difference, whereas rejection at $\alpha = 0.05$ meant indifferent increase/decrease. Rejection of H_0 at $\alpha = 0.01$ and 0.001 meant significant and highly significant increase/decrease of solar hemispheric transmittance, respectively.

Results. In Table VII, the threshold temperature, temperature interval of the major switching process, mean of solar hemispheric and diffuse transmittance below and above the threshold temperature (empirical standard deviation[45] in brackets), and test variable t_d are summarized for TSFD based on thermoplastic matrix. Solar hemispheric transmittance changed from between 36.7 and 80.7% to values between 53.3 and 83.5% upon exceeding the threshold temperature. Solar diffuse transmittance ranged from 15.2 to 44.1% at room temperature. Upon exceeding the threshold temperature it changed to values between 31.4 and 65.9%.

Whereas TSFD M3A21 displayed an indifferent increase in solar hemispheric transmittance, layers M2A2 and M3A20 exhibited an insignificant change in solar hemispheric transmittance. Compared to other layers, the standard deviation of solar hemispheric and diffuse transmittance above the threshold temperature for layer M2A2 was very high (around 13.6 and 12.0%, respectively). In general, high standard deviation of solar hemispheric transmittance above the threshold temperature is an indication for sample inhomogeneity. At least a significant increase in solar hemispheric transmittance was evident for layers M1A1, M1A2, M1A11, and M2A6. The increase of solar hemispheric transmittance attained for these layers violated predictions from refractive index data. This is attributed to different coefficients of thermal expansion (CTE) of matrix and additive most likely. For example CTE for PMMA and paraffin are in the range of 6–8 $\times$ 10^{-5} and 0.7–1.1 $\times$ 10^{-3} K^{-1}, respectively.[46,47] Upon cooling during manufacturing, the higher CTE of paraffin leads to more intense contraction of the embedded additive domains compared to surrounding matrix PMMA. Combined with limited adhesion at the interface of matrix and additive, vacuoles are formed. The high refractive index difference between matrix and vacuoles ($n = 1$) yields intense scattering and thus a low solar hemispheric transmittance at room temperature. Upon heating and especially upon melting the additive expands and fills the cavity completely. Thus, the refractive index difference at the scattering interface is reduced, yielding an increase in solar hemispheric transmittance. Detailed investigations concerning layer morphology and to confirm this assumptions are currently under way. On the contrary, a highly significant decrease in solar hemispheric transmittance from 78.9 to 63.3% was evident for layer M2A11 upon exceeding the threshold temperature. At temperatures below

Table VIII. Threshold Temperature T_{th}, Major Switching Interval ΔT_{major}, Mean of Solar Hemispheric and Diffuse Transmittance Below and Above the Threshold Temperature of TSFD Based on UV-Curable Resin Matrix (Empirical Standard Deviation in Brackets), and Test Variable t_d

			Solar transmittance below threshold temperature (%)		Solar transmittance above threshold temperature (%)			
TSFD	T_{th} (°C)	ΔT_{major} (°C)	Hemisph.	Diffuse	Hemisph.	Diffuse	t_d	Remarks
M4A1	30	25	63.5 (1.4)	56.1 (0.4)	75.4 (6.1)	73.7 (5.6)	3.26	Indifferent incr.
M4A2	70	10	76.6 (0.4)	26.1 (3.1)	80.0 (3.0)	48.6 (1.4)	2.24	Insignificant
M4A3	50	10	79.2 (2.5)	55.6 (6.3)	70.9 (1.7)	61.8 (2.9)	−11.9	Significant decr.
M4A5	70	10	80.5 (1.1)	42.1 (2.5)	77.7 (3.0)	73.5 (2.1)	−1.52	Insignificant
M4A6	50	15	71.0 (19.3)	51.3 (3.7)	81.3 (1.6)	78.2 (1.0)	0.99	Insignificant
M4A7	60	10	83.3 (1.3)	40.7 (9.3)	85.0 (0.2)	69.8 (4.0)	2.19	Insignificant
M4A8	50	10	75.9 (3.4)	51.2 (2.8)	69.0 (5.6)	61.5 (3.8)	−5.36	Indifferent decr.
M4A9	60	15	74.7 (11.3)	53.2 (2.2)	75.9 (0.8)	61.7 (4.6)	0.21	Insignificant
M4A10	70	10	80.4 (1.0)	42.7 (3.3)	78.4 (3.2)	71.5 (1.2)	−1.21	Insignificant
M5A1	45	20	82.2 (1.1)	52.5 (1.0)	84.0 (1.0)	81.4 (1.0)	6.22	Indifferent incr.
M5A2	55	25	74.7 (9.4)	43.6 (3.3)	82.2 (1.2)	71.5 (2.3)	1.23	Insignificant
M5A3	55	>60	83.1 (1.2)	41.5 (8.2)	75.0 (19.4)	28.1 (14.7)	−0.68	Insignificant; irreversible degradation
M5A4	50	10	69.4 (6.1)	53.6 (2.2)	78.5 (0.7)	75.9 (0.4)	2.85	Insignificant
M5A5	65	15	81.1 (1.0)	24.2 (5.9)	81.9 (1.8)	67.7 (2.8)	0.80	Insignificant
M5A6	40	25	82.2 (1.3)	33.1 (4.8)	82.4 (1.0)	77.2 (1.9)	0.12	Insignificant
M5A7	60	10	81.1 (2.7)	39.2 (8.8)	84.5 (0.9)	28.3 (7.1)	3.17	Indifferent incr.
M5A8	50	15	77.9 (0.5)	37.2 (3.9)	73.2 (0.7)	66.5 (0.8)	−38.8	Highly sign. decr.
M5A9	65	10	80.4 (1.7)	64.8 (5.1)	78.0 (1.0)	68.6 (3.3)	−2.74	Insignificant
M5A10	70	10	82.8 (0.5)	17.5 (4.9)	82.9 (1.2)	68.4 (2.7)	0.20	Insignificant
M6A1	45	10	62.2 (3.5)	54.2 (2.7)	77.3 (1.6)	74.6 (1.8)	8.15	Significant incr.
M6A2	55	20	69.9 (10.2)	42.9 (11.3)	80.4 (2.1)	72.6 (1.5)	1.89	Insignificant
M6A3	50	10	72.3 (4.6)	53.5 (7.4)	59.6 (3.7)	54.0 (2.7)	−27.1	Highly sign. decr.
M6A10	65	15	72.2 (3.3)	64.3 (2.3)	65.3 (2.0)	64.2 (2.0)	−8.07	Significant decr.
M7A1	45	10	69.6 (8.3)	48.9 (7.2)	82.9 (1.5)	79.1 (1.9)	2.69	Insignificant
M7A2	60	15	63.4 (3.4)	45.0 (2.1)	81.7 (1.2)	72.8 (0.8)	7.06	Significant incr.
M7A3	50	10	78.8 (1.0)	51.2 (0.9)	65.3 (2.1)	57.3 (1.2)	−17.5	Significant decr.
M7A4	50	20	73.1 (4.9)	50.9 (0.7)	75.5 (0.9)	70.6 (0.9)	0.70	Insignificant
M7A5	75	5	81.0 (0.6)	33.5 (6.6)	78.7 (1.8)	74.0 (2.8)	−3.19	Indifferent decr.
M7A6	45	20	80.3 (2.2)	49.2 (4.3)	81.0 (0.8)	77.2 (0.8)	0.56	Insignificant
M7A7	65	5	84.5 (0.6)	20.0 (8.4)	83.7 (0.7)	51.2 (4.4)	−2.10	Insignificant
M7A8	50	15	76.4 (1.1)	48.9 (3.6)	67.2 (0.6)	61.7 (0.5)	−12.0	Significant decr.
M7A9	45	30	80.5 (1.8)	63.5 (1.3)	75.2 (0.3)	70.1 (0.8)	−6.18	Indifferent decr.
M7A10	60	20	80.6 (1.2)	34.9 (4.0)	78.8 (2.6)	72.9 (1.5)	−2.09	Insignificant

75°C the hemispheric transmittance decreased rather smoothly, whereas between 75 and 100°C the reduction was steeper. The gradual switching process was in agreement with the broad melting range and the gradual refractive index change of the thermotropic additive A11, detected by DSC and refractometry, respectively. Probably no vacuoles were formed for material combination M2A11. This was likely to be attributed to the epoxy-moiety in additive A11, which is able to form covalent bonds with amide-groups in PA (M2).[48]

In Table VIII, the threshold temperature, temperature interval of the major switching process, mean of solar hemispheric and diffuse transmittance below and above the threshold temperature (empirical standard deviation[45] in brackets) and test variable t_d are summarized for TSFD based on UV-curable resin matrix. Solar hemispheric transmittance changed from between 62.2 and 84.5% to values between 59.6 and 85.0% upon exceeding the threshold temperature. Solar diffuse transmittance ranged from 17.5 to 64.8% at room temperature. Upon

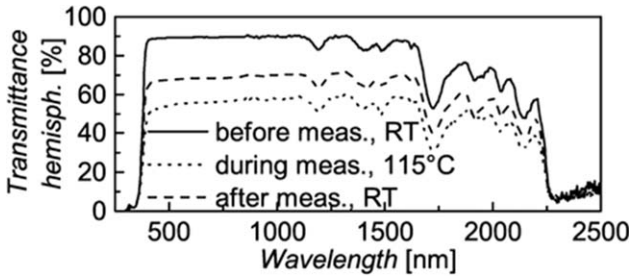

Figure 4. Hemispheric transmittance of Sample 1 of M5A3 before acquisition of solar-optical properties of layers formulated with additive A3 as a function of temperature (solid line), during acquisition (dotted line), and after acquisition (dashed line).

exceeding the threshold temperature it changed to values between 28.1 and 81.4%.

Materials M6A1 and M7A2 exhibited a significant increase of solar hemispheric transmittance above the switching threshold. An indifferent increase was evident for layers M4A1, M5A1, and M5A7. Layers M4A2, M4A6, M5A2, M5A4, M6A2, and M7A1 showed an increase in mean solar hemispheric transmittance upon switching. However, high standard deviation of transmittance change yielded these changes to be insignificant. High standard deviation of transmittance change indicates low sample homogeneity. The increase of solar hemispheric transmittance detected for these layers violated predictions from refractive index data. The observed increase in transmittance instead of the theoretically suggested decrease was attributed to vacuoles (refractive index $n = 1$) which are probably formed at the perimeter of the scattering domains, yielding intense scattering at ambient conditions. Suggested vacuole formation mechanism is slightly different for these systems compared to TSFD based on thermoplastics. During curing procedure components of prefabricated mixtures of UV-curable resin and thermotropic additive are exposed to radiation yielding crosslinking reaction in the matrix and heating up of thermotropic mixture due to absorption. Upon cooling, the embedded additive particles contract more intense than the surrounding matrix due to higher CTE of thermotropic additive compared to the matrix material. Combined with limited adhesion at the interface of matrix and additive, vacuoles are formed. The increase of solar hemispheric transmittance upon heating is ascribed to the same mechanisms as already described above. Solar hemispheric transmittance changes between −2.8 and 2.4% achieved for layers M4A5, M4A7, M4A9, M4A10, M5A5, M5A6, M5A9, M5A10, M7A4, M7A6, M7A7, and M7A10 were insignificant. However, samples of M4A9 showed strongly differing solar hemispheric transmittance at room temperature (Sample 1: 82.0%; Sample 2: 80.3%; Sample 3: 61.6%), whereas transmittance changed to 75.9% upon heating. Sample 3 probably contains vacuoles, whereas Samples 1 and 2 do not. An indifferent decrease of solar hemispheric transmittance was detected for layers M4A8, M7A5, and M7A9. Solar hemispheric transmittance decrease by −2.3 to −6.9% was evident for these materials. Solar hemispheric transmittance reduction by −4.7 to −13.5% was attained for layers M4A3, M5A3, M5A8, M6A3, M6A10, M7A3, and M7A8. The *t*-test revealed these changes to be at least significant for TSFD M4A3, M5A8, M6A3, M6A10, M7A3, and M7A8. However, transmittance change for layer M5A3 was insignificant. Investigations revealed incoherent switching behavior of the three samples investigated: The best performing sample, which was one out of three replicates of M5A3, exhibited a change in solar hemispheric transmittance from 84.4 to 52.7%. However, the switching was partially irreversible. In Figure 4, the hemispheric transmittance of Sample 1 of layer M5A3 is displayed at room temperature (solid line) and at 115°C (dotted line). A distinct reduction of transmittance over the entire wavelength range between 375 and 2250 nm was observed upon heating. The dashed line represents a spectrum recorded after cooling to ambient temperature and sufficient equilibration time (hemispheric transmittance 64.7%). The area between the dashed and the dotted line may represent the reversible portion of the process. It may be attributed to solidification of the additive and thus reduction of refractive index difference of matrix and additive. The area between the solid and the dashed line corresponds to an irreversible process. The irreversible portion may be ascribed to formation of crack-like structures inside the sample occurring after exposure to elevated temperatures. These cracks (refractive index $n = 1$) may act as persistent scattering domains, thus yielding a permanent reduction of hemispheric transmittance. Interestingly, the two other samples produced from material M5A3 displayed an increase of hemispheric solar transmittance upon heating. As a consequence standard deviation of hemispheric solar transmittance above the threshold temperature given in Table VIII was reasonable high (19.4%). Nevertheless, hazy areas were also observed for these layers even though in less lateral extension than for Sample 1. These specimens displayed minor irreversible portion of transmittance change as indicated by hemispheric transmittance of 82.0 or 82.9% and 78.1 or 76.6% before and after the heating cycle, respectively.

Figure 5 displays solar hemispheric transmittance of TSFD as a function of the absolute of refractive index difference of matrix and additive below and above the switching threshold. Merely matrix/additive combinations yielding a reduction in hemispheric solar transmittance above the switching threshold are considered. The data scatter reveals a slight trend: The higher the refractive index difference between matrix and additive, the lower the solar hemispheric transmittance. This indicates clearly, that refractometry is an appropriate tool for material

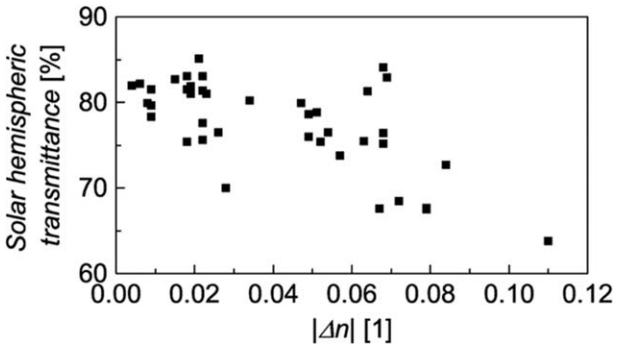

Figure 5. Solar hemispheric transmittance of selected TSFD as a function of the absolute of refractive index difference of matrix and additive.

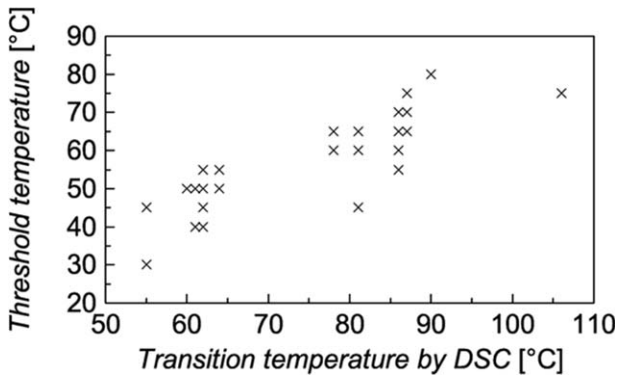

Figure 6. Threshold temperatures of TSFD detected by UV/Vis/NIR spectrometry as a function of transition temperature of corresponding thermotropic additives detected by DSC.

preselection for formulation of TSFD. Nevertheless, exact prediction of transmittance reduction from refractive index data as a function of temperature of matrix and additive is not possible due to the significant effect of TSFD morphology (scattering domain size and shape) on scattering performance.[5,49,50]

With regard to refractive index data every formulated TSFD has the potential to display a reduction of solar hemispheric transmittance upon exceeding the threshold temperature in principle. However, morphology of TSFD has a significant effect on switching characteristics of a TSFD also.[5,15,49,50] Thus, observed increase of solar hemispheric transmittance of several TSFD might be ascribed to inappropriate sample morphology (e.g., vacuoles).

Detected threshold temperatures ranged from 30 to 75°C. For several of these materials, switching interval was rather narrow within a frame of 5–10°C. A more transient transition with a broader switching interval between 15 and 30°C was attained for TSFD M4A1, M4A6, M4A9, M5A1, M5A2, M5A5, M5A6, M5A8, M6A2, M6A10, M7A2, M7A4, M7A6, M7A8, M7A9, and M7A10. The transition interval of M5A3 was >60°C. In Figure 6, the threshold temperatures of TSFD detected by UV/Vis/NIR spectrometry are depicted as a function of transition temperature of the corresponding thermotropic additives detected by DSC. A good correlation is discernible which is in agreement with findings by Resch et al.[15,51] Thus, DSC is an appropriate tool for selection of thermotropic additives to tune the threshold temperature of TSFD.[15,51] However, attempts to determine the DSC thermograms of formulated TSFD revealed no reasonable results due to the low concentration (5 wt %) of the thermotropic additives and hence low sensibility of DSC with regard to thermal transitions of the thermotropic additives.

CONCLUSIONS AND OUTLOOK

In this article, a systematic material formulation strategy was applied to establish thermotropic systems with fixed domains (TSFD) providing efficient overheating protection. Systematic preselection of matrix materials and thermotropic additives was carried out utilizing thermoanalytical methods and refractometry. Promising TSFD were formulated based on assessment of refractive index match of matrix and additive. Whereas most TSFD were producible properly, several TSFD based on thermoplastics lacked miscibility of matrix and additive due to high viscosity differences. Investigations revealed a good correlation of transition temperature of the thermotropic additives detected by DSC and the threshold temperature of the layers formulated therewith, thus enabling adjustment of switching threshold by selecting adequate thermotropic additives with transition temperature in the desired range (e.g., for window application or solar thermal collectors). A close correlation of refractive index difference and measured solar transmittance was observed, which is in good agreement with theoretical considerations.[5] Thus refractometry is an appropriate tool for preselection of candidate combinations of matrix materials and thermotropic additives. A little number of formulated TSFD exhibited no thermoresponsive behavior. Other materials were showing either an increase or a decrease of hemispheric solar transmittance upon exceeding the switching threshold. In general, the overheating protection potential of the TSFD formulated within this study is limited. Recent studies ascribe the limited overheating protection potential of TSFD to inappropriate size and shape of scattering domains.[49,50] Thus, a related article[17] will deal with a comprehensive characterization of morphology with specific focus on scattering domain shape and size. Subsequently, structure-property-relationships will be established and optimization strategies will be presented.

ACKNOWLEDGMENTS

This research project was funded by the State Government of Styria, Department Zukunftsfonds (Project number 5019). The efforts in determination of solar-optical properties of parts of the formulated TSFD by Alexander Klutz (Polymer Competence Center Leoben GmbH, PCCL, Leoben, AT), Astrid Rauschenbach (PCCL) and Andrea Schmid (Department of Polymer Engineering and Science, University of Leoben, AT) and support concerning UV equipment by Sandra Schlögl (PCCL) and compounding of materials with thermoplastic matrix by Karl Schnetzinger (APC Advanced Polymer Compounds, Gai, AT) are gratefully acknowledged. Furthermore, the authors wish to acknowledge the contributions of Arkema GmbH (Düsseldorf, DE), Baerlocher GmbH (Unterschleissheim, DE), Bayer Materials Science AG (Leverkusen, DE), Biesterfeld Interowa GmbH & Co. KG (Wien, AT), Brenntag CEE GmbH (Traun, AT), Chemson Polymer Additive AG (Arnoldstein, AT), Allnex Belgium SA/NV (formerly Cytec Surface Specialities Inc.; Drogenbos, BE), DuPont de Nemours (Deutschland) GmbH (Neu-Isenburg, DE), Evonik Degussa GmbH, High Performance Polymers (Marl, DE), Evonik Röhm GmbH (Darmstadt, DE), HDS-Chemie HandelsgesmbH (Wien, AT), Sasol Wax GmbH (Hamburg, DE), and Senoplast Klepsch GmbH (Piesendorf, AT).

REFERENCES

1. Nitz, P.; Hartwig, H. *Sol. Energy* **2005**, *79*, 573.
2. Seeboth, A.; Schneider, J.; Patzak, A. *Sol. Energy Mater. Sol. Cells* **2000**, *60*, 263.
3. Nitz, P.; Wagner, A. *BINE Themeninfo* **2002**, I/02, 1.

4. Wallner, G. M.; Resch, K.; Hausner, R. *Sol. Energy Mater. Sol. Cells* **2008**, *92*, 614.
5. Nitz, P. Optical modelling and characterisation of thermotropic systems. Dissertation, Albert-Ludwigs-Universität, Freiburg i.B., **1999**.
6. Inoue, T. *Energy Build.* **2003**, *35*, 463.
7. Yao, J.; Zhu, N. *Build. Environ.* **2012**, *49*, 283.
8. Hartwig, H. Concepts for the Integration of Self Regulating Thermotropic Layers into Modern Buildings Envelopes for Passive Solar Energy Utilization, Dissertation, Technische Universität, München,, **2003**.
9. Raicu, A.; Wilson, H.R.; Nitz, P.; Platzer, W.; Wittwer, V.; Jahns, E. *Sol. Energy* **2002**, *72*, 31.
10. Manz, H.; Menti, U.-P. *Renew. Energy* **2012**, *37*, 226.
11. Resch, K.; Weber, A. *Berg- Huettenmaenn. Monatsh.* **2011**, *156*, 429.
12. Resch, K.; Wallner, G. M. *Sol. Energy Mater. Sol. Cells* **2009**, *93*, 119.
13. Nitz, P.; Ferber, J.; Stangl, R.; Wilson, H. R.; Wittwer, V. *Sol. Energy Mater. Sol. Cells* **1998**, *54*, 297.
14. Muehling, O.; Seeboth, A.; Haeusler, T.; Ruhmann, R.; Potechius, E.; Vetter, R. *Sol. Energy Mater. Sol. Cells* **2009**, *93*, 1510.
15. Resch, K.; Wallner, G. M.; Hausner, R. *Sol. Energy* **2009**, *83*, 1689.
16. Resch, K.; Wallner, G. M.; Lang, R. W. *Macromol. Symp.* **2008**, *265*, 49.
17. Weber, A.; Schmid, A.; Resch, K. *J. Appl. Polym. Sci.*, **2013**, DOI: 10.1002/app.39910.
18. Ehrenstein, G. W.; Pongratz, S. Beständigkeit von Kunststoffen; Hanser: München, **2007**.
19. Seferis, J. C. In Polymer Handbook; Brandrup, J., Immergut, E. H., Grulke, E. A., Eds.; Wiley: New York, **1999**, pp VI/571–VI/582.
20. Ehrenstein, G. W.; Riedel, G.; Trawiel, P. Praxis der thermischen Analyse von Kunststoffen; Hanser: München, **2003**.
21. Schiebener, P.; Straub, J.; Levelt Sengers, J. M. H.; Gallagher, J. S. *J. Phys. Chem. Ref. Data* **1990**, *19*, 677.
22. Hellerich, W.; Harsch, G.; Haenle, S. Werkstoff-Führer Kunststoffe: Eigenschaften, Prüfungen, Kennwerte; Hanser: München, **2004**.
23. El Fadli, K. I.; Cerveny, R. S.; Burt, C. C.; Eden, P.; Parker, D.; Brunet, M.; Peterson, T. C.; Mordacchini, G.; Pelino, V.; Bessemoulin, P.; Stella, J. L.; Driouech, F.; Wahab, M. A.; Pace, M. B. *Bull. Am. Meteor. Soc.* **2013**; *94*, 199.
24. Demtröder, W. Experimentalphysik 2: Elektrizität und Optik; Springer: Berlin, **2006**.
25. Hammami, A.; Mehrotra, A. K. *Fuel* **1995**, *74*, 96.
26. Luyt, A.; Krupa, I. *Thermochim. Acta* **2008**, *467*, 117.
27. Briard, A.; Bouroukba, M.; Petitjean, D.; Hubert, N.; Moise, J.; Dirand, M. *Fuel* **2006**, *85*, 764.
28. Egorov, V. M.; Marikhin, V. A.; Myasnikova, L. P. *Polym. Sci. Ser. A Polym. Phys.* **2007**, *49*, 1366.
29. Ventola, L.; Cuevas-Diarte, M. A.; Calvet, T.; Angulo, I.; Vivanco, M.; Bernar, M.; Bernar, G.; Melero, M.; Mondieig, D. *J. Phys. Chem. Solids* **2005**, *66*, 1668.
30. Gu, W. *Anal. Chem.* **1993**, *65*, 827.
31. Vereecken, J.; Meeussen, W.; Foubert, I.; Lesaffer, A.; Wouters, J.; Dewettinck, K. *Food Res. Int.* **2009**, *42*, 1415.
32. O'Laughlin, R.; Sachs, C.; Brittain, H.; Cohen, E.; Timmins, P.; Varia, S. *J. Soc. Cosmet. Chem.* **1989**, *40*, 215.
33. Chen, J.; Chen, H.; Cui, S.; Xue, B.; Tian, J.; Achilefu, S.; Gu, Y. *J. Mater. Chem.* **2012**, *22*, 5770.
34. Belitz, H.-D.; Grosch, W.; Schieberle, P. Lehrbuch der Lebensmittelchemie; Springer: Berlin, **2008**.
35. Hartel, R. W. Crystallization in Foods; Aspen Publishers: Gaithersburg, MD, **2001**.
36. Lavigne, F.; Bourgeaux, C.; Ollivon, M. *J. Phys. IV* **1993**, *3*, 137.
37. Oh, J.-H.; McCurdy, A.; Clark, S.; Swanson, B. *J. Food Sci.* **2002**, *67*, 2911.
38. Eloundou, J. P.; Girard-Reydet, E.; Gérard, J.-F.; Pascault, J.-P. *Polym. Bull.* **2005**, *53*, 367.
39. IFA. GESTIS-Stoffdatenbank: Naphthalin; 2012. Available at: http://gestis.itrust.de/nxt/gateway.dll/gestis_de/015510.xml?f=templates$fn=default.htm$3.0, accessed March 22, 2012.
40. Cabeza, L.; Castell, A.; Barreneche, C.; Gracia, A. de ; Fernández, A. *Renew. Sustain. Energy Rev.* **2011**, *15*, 1675.
41. Sharma, A.; Tyagi, V.; Chen, C.; Buddhi, D. *Renew. Sustain. Energy Rev.* **2009**, *13*, 318.
42. Sachs, L. Angewandte Statistik: Anwendung statistischer Methoden; Springer: Berlin, **2004**.
43. Montgomery, D. C. Design and Analysis of Experiments; Wiley: Hoboken, NJ, **2009**.
44. Kleppmann, W. Taschenbuch Versuchsplanung: Produkte und Prozesse optimieren; Hanser: München, **2009**.
45. Bartsch, H.-J. Taschenbuch mathematischer Formeln für Ingenieure und Naturwissenschaftler; Hanser: München, **2011**.
46. Baur, E.; Brinkmann, S.; Osswald, T. A.; Schmachtenberg, E. Saechtling-Kunststoff-Taschenbuch; Hanser: München, **2007**.
47. Schimmelpfennig, M.; Weber, K.; Kalb, F.; Feller, K.-H.; Butz, T.; Matthäi, M. In Jahrbuch für den Praktiker 2007: Handbuch für Rohstoff und Formulierung Industrie, Gewerbe und Haushalt; Ziolkowsky, B., Ed.; Verlag für chemische Industrie: Augsburg, **2007**; Vol. *50*, pp 417–429.
48. Koning, C.; van Duin, M.; Pagnoulle, C.; Jerome, R. *Prog. Polym. Sci.* **1998**, *23*, 707.
49. Resch, K.; Wallner, G. M. *Polym. Adv. Technol.* **2009**, *20*, 1163.
50. Weber, A.; Resch, K. *J. Polym. Res.* **2012**, *19*, 1.
51. Resch, K.; Wallner, G. M. In Proceedings of ISES Solar World Congress 2007; Goswami, D. Y., Zhao, Y., Eds.; Springer: Berlin, **2007**; pp 541–545.